



HAL
open science

Active interseismic shallow deformation of the Pingting terraces (Longitudinal Valley – Eastern Taiwan) from UAV high-resolution topographic data combined with InSAR time series

Benoît Deffontaines, Kuo-Jen Chang, Johann Champenois, Bénédicte Fruneau, Erwan Pathier, Jyr-Ching Hu, Shih-Ting Lu, Yen-Chiu Liu

► To cite this version:

Benoît Deffontaines, Kuo-Jen Chang, Johann Champenois, Bénédicte Fruneau, Erwan Pathier, et al.. Active interseismic shallow deformation of the Pingting terraces (Longitudinal Valley – Eastern Taiwan) from UAV high-resolution topographic data combined with InSAR time series. *Geomatics, Natural Hazards and Risk*, 2016, 8 (1), pp.120-136. 10.1080/19475705.2016.1181678 . hal-02882441

HAL Id: hal-02882441

<https://hal.science/hal-02882441>

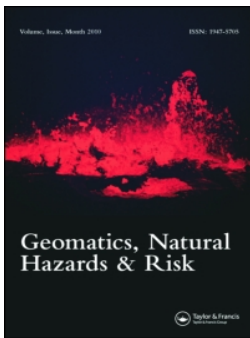
Submitted on 23 Nov 2021

HAL is a multi-disciplinary open access archive for the deposit and dissemination of scientific research documents, whether they are published or not. The documents may come from teaching and research institutions in France or abroad, or from public or private research centers.

L'archive ouverte pluridisciplinaire **HAL**, est destinée au dépôt et à la diffusion de documents scientifiques de niveau recherche, publiés ou non, émanant des établissements d'enseignement et de recherche français ou étrangers, des laboratoires publics ou privés.



Distributed under a Creative Commons Attribution 4.0 International License



Active interseismic shallow deformation of the Pingting terraces (Longitudinal Valley – Eastern Taiwan) from UAV high-resolution topographic data combined with InSAR time series

Benoît Deffontaines, Kuo-Jen Chang, Johann Champenois, Bénédicte Fruneau, Erwan Pathier, Jyr-Ching Hu, Shih-Ting Lu & Yen-Chiu Liu

To cite this article: Benoît Deffontaines, Kuo-Jen Chang, Johann Champenois, Bénédicte Fruneau, Erwan Pathier, Jyr-Ching Hu, Shih-Ting Lu & Yen-Chiu Liu (2017) Active interseismic shallow deformation of the Pingting terraces (Longitudinal Valley – Eastern Taiwan) from UAV high-resolution topographic data combined with InSAR time series, *Geomatics, Natural Hazards and Risk*, 8:1, 120-136, DOI: [10.1080/19475705.2016.1181678](https://doi.org/10.1080/19475705.2016.1181678)

To link to this article: <https://doi.org/10.1080/19475705.2016.1181678>



© 2016 The Author(s). Published by Informa UK Limited, trading as Taylor & Francis Group



Published online: 25 Jul 2016.



Submit your article to this journal [↗](#)



Article views: 1251



View related articles [↗](#)



View Crossmark data [↗](#)



Citing articles: 11 View citing articles [↗](#)

Active interseismic shallow deformation of the Pingting terraces (Longitudinal Valley – Eastern Taiwan) from UAV high-resolution topographic data combined with InSAR time series

Benoît Deffontaines ^{a,b}, Kuo-Jen Chang^{b,c}, Johann Champenois^{d,b}, Bénédicte Fruneau^{b,d}, Erwan Pathier^{b,e}, Jyr-Ching Hu^{b,f}, Shih-Ting Lu^g and Yen-Chiu Liu^g

^aUniversité Paris-Est, LaSTIG/LAREG, IGN, UPEM, UDD, 77454 Marne-la-Vallée, France; ^bLIA D3E (From Deep Earth to Extreme Event) France-Taiwan; ^cDepartment of Civil Engineering, National Taipei University of Technology, Taipei, ROC; ^dUniversité Paris-Est, LaSTIG/MATIS, IGN, UPEM, 77454 Marne-la-Vallée, France; ^eInstitut des Sciences de la Terre, Université Joseph Fourier, Grenoble, France; ^fDepartment of Geosciences, National Taiwan University, Taipei, Taiwan, ROC; ^gCentral Geological Survey, MOEA, Taipei, Taiwan, ROC

ABSTRACT

We focus herein on the location, characterization and the quantification of the most active structural feature of Taiwan: the Longitudinal Valley Fault that corresponds to the suture in between the Philippine and Eurasian Plates. In order to determine and monitor its present inter-seismic deformation, we focus on the Pingting Terraces area, situated in the South Longitudinal Valley (Eastern Taiwan). We first determine the structural geometry issued from both photo-interpretation deduced from new unmanned aerial vehicle (UAV) high-resolution Digital Terrain Model data that we acquired (34.78 km² with 7.73 cm ground sampling distance), combined with geological field work. In order to characterize and quantify the present deformational patterns over the Pingting terraces, we used an InSAR time series Interferometry algorithm (MT-InSAR) applied to nine L-band SAR images from ALOS satellite acquired over the period 2007–2010. The unprecedented density of measurements (about 120 points per km² for a total of 6,400 points) gives a continuous overview of the inter-seismic shallow deformation. The structural geometry combined with the mean velocity map (MT-InSAR) reveals two clear active faults situated above the scarps of the Pingting terraces and responsible for up to 7 and 20 mm/yr velocity offset along the radar line of sight. A temporal analysis of the deformation is performed with one measurement at each SAR acquisition date, giving major improvements in the characterization and quantification of the Longitudinal Valley active Fault trace.

ARTICLE HISTORY

Received 1 December 2015
Accepted 14 April 2016

KEYWORDS

UAV; high-resolution Digital Terrain Model; SAR interferometry; persistent scatterers; small baseline; interseismic deformation; Longitudinal Valley Fault; Pingting terraces; Eastern Taiwan

1. Introduction

How to locate, characterize and quantify the active deformation of the southern Longitudinal Valley Fault (LVF) in eastern Taiwan which is the most active tectonic feature of the Taiwan orogen (Figure 1(a))? The Longitudinal Valley is the outcropping active tectonic suture in between the ongoing collision of the continental Eurasian margin and the oceanic and volcanic Philippine Sea plate (e.g. Ho 1986; Angelier et al. 1997; Malavieille et al. 2002). This narrow elongated valley, N020°E trending and 120 km long, separates the mainly volcanic deposits of the Coastal Range

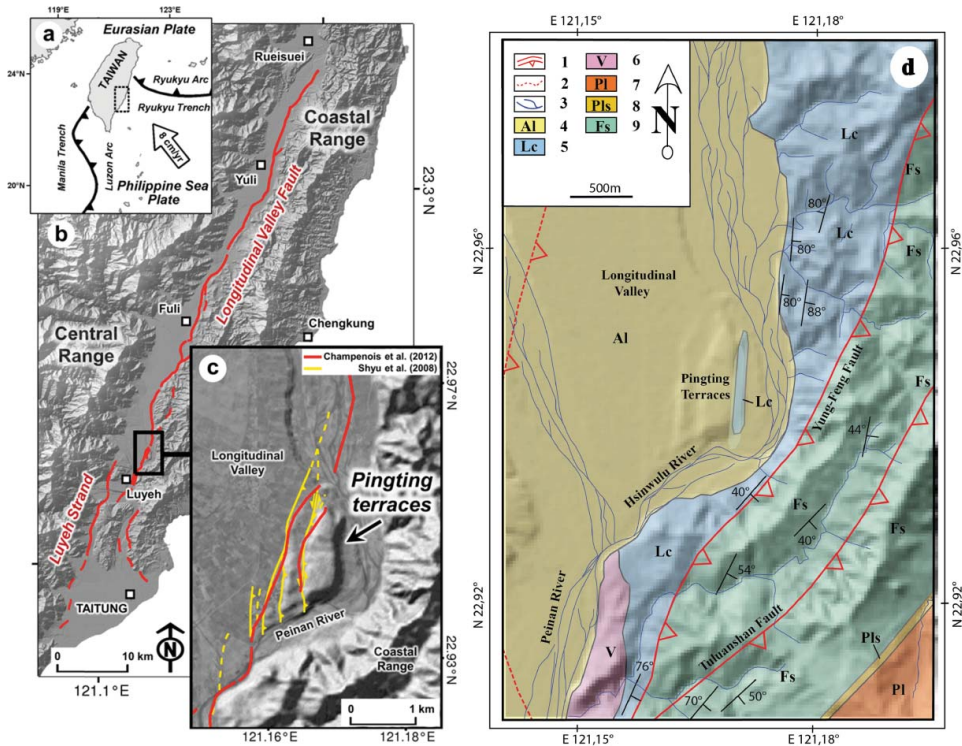


Figure 1. (left (a)) Tectonic setting of Taiwan. Taiwan results from the ongoing collision between the Eurasian and the Philippine Sea Plates. The black arrow indicates the direction of convergence between these two plates with an estimated rate of about 8 cm per year (Seno et al. 1993; Yu & Kuo 2001) (black dashed frame: location of (b)). (b) Active tectonic map of the south Longitudinal Valley (Eastern Taiwan). The red lines show major active fault traces located in the Longitudinal Valley (Champenois et al. 2012): the Longitudinal Valley Fault and the Luyeh Strand – black frame: location of (c). In background, shaded relief is extracted from the Taiwan 40 m Digital Terrain Model. (c) Faults map of the Pingting Terraces. The red lines show fault map derived from persistent scatterers SAR interferometry analysis (Champenois et al. 2012), while the yellow lines show active fault map derived from geomorphological analysis (Shyu et al. 2008). Fault traces are superimposed on the 40 m ground resolution shaded relief map. ((d) right figure) Known geology from the 1/100,000 scale geological map of the coastal range (Wang and Chen, 1993). One may note the location and the basic inferred geometry of the three faults (Longitudinal Valley, Yungfeng, and Tuluanshan Faults). (1) Fault, (2) inferred fault, (3) drainage network, (4) alluviums, (5) Lichi Mélange, (6) andesitic block within the Lichi Mélange, (7) Paliwan Formation Conglomerate facies, (8) Paliwan Formation, and (9) Fanshuliao formation.

(CoaR, below) to the east and the Metamorphic Central Range (MCenR, below) to the west (Figure 1(b)). According to sparse GPS continuous measurements, about 30% of the 8.2 cm/yr of the present plate convergence and shortening occurs across the Longitudinal Valley (Yu & Kuo 2001) which reveal the importance of this active structural feature. In order to decipher the outcropping geometry and the inter-seismic activity of the LVF, we focus herein in its southern part, in between the Peinanshan (north of Taitung city) and the Tapo-Chihshang area (Angelier et al. 1997; Lee et al. 2001, 2003; Shyu et al. 2008), where the two Pingting terraces are well preserved due to the eastern avulsion of the Hsinwulu river within the soft and clayey Lichi Mélange (e.g. Barrier & Muller 1984; Chang et al. 2000; Huang et al. 2008; Chi et al. 2014). This area represents a case geomorphic example in Taiwan of super-imposition of active tectonics and river incision within the dark blue, soft and deep-offshore clayey and blocky Lichi Mélange (Figure 1).

From a geological point of view several published geological maps had been settled since Hsu (1956). The last one of the Central Geological Survey (Wang & Chen 1993) highlights the existing lithologies and locally oblique lithologic structures boundaries to the new acquired detailed topography. Therefore, the latter acquired during this study, leads us to up-date precisely geological

mapping as well as the structural geology. The different major geological units are the Lichi Mélange (Lc) which is composed of dark blue colour offshore deep sea clays highly deformed and bearing big blocks such as the andesitic one in the south of the studied area (V, [Figure 1\(d\)](#)). Two thrust faults (Yung-Feng and Tuluanshan Faults) affect the Fanshuliao formation (Fs) that over-thrust the Lichi Mélange that correspond to volcanic strata, and cinerites of the Luzon volcanic arc. The overlying Paliwan facies begins with a characteristic conglomerate (Pls) then sandstones that both belong to the alluvial deposits resulting from the erosion of the MCenR (Eurasian continental margin – Hsu 1956; Teng & Lo 1985).

We herein propose to precise (1) the detailed structural geometry of the place by both using classical photo-interpretation of high-resolution Digital Terrain Model (DTM) acquired through unmanned aerial vehicle (UAV) and validated by field studies, and (2) to determine the activity of the LVF branches by adding information derived by the PALSAR – ALOS1 time series interferometry in between 2007 and 2010.

2. UAV's high-resolution topographic data

2.1. Acquisition and methodology

A UAV, commonly known as a 'drone' is an aircraft without human pilot on board. The UAV used in this study is a modified version of the already-available Skywalker X5 and X8 fixed-wing aircraft reinforced by carbon fibre rods. The drone is launched by hand, flies and takes photos autonomously, then glides and/or parachutes back down to the ground by using a pre-programmed flight plans organized by ground control system, and controlled by the ground control station and remote controller. The autopilot system is composed and modified from the open source APM (ArduPilot Mega 2.6 autopilot) firmware and open source software Mission Planner, transmitted by ground-air XBee radio telemetry. In order to generate high-resolution digital terrain model (DTM) and mosaic orthorectified images, a total of 6275 photos were gathered by Sony DSC-QX100 and Sony ILCE-QX1 cameras mounted on X5 and X8, respectively. The total scan covered an area of 34.78 km² with 7.73 cm ground sampling distance (GSD). The coverage of the adjacent photos is kept at least for 80% overlap and 60% sidelap. The datasets generated in this study are the orthorectified mosaic image and DTMs, with a grid spacing of 7.73 cm. To get these results, the raw images were processed by Pix4Dmapper and Smart3Dcapture software mutually. In most of the scanned area, the number of overlapping images computed for each pixel of the orthomosaic image is higher than 5 photos. The generated point cloud is as high as 698 million points for the study area. Prior to the morpho-tectonic analysis, the quality of the dataset needs to be evaluated. The techniques and the quality of the digital surface models (DSMs) can be controlled within a maximum error smaller than 40 cm (ΔZ) following our previous work where we compared such methodology with the ground levelling profiles and airborne LiDAR data in Hualien county, Taiwan (Huang & Chang 2014). The same methodology is used in this study to gather and produce the datasets.

The principle of the method used in this study is to analyse several photos of a static object taken from different viewpoints, then detect pixels corresponding to a same physical points, automatically. From many such correspondences, the orientation of photos is then calculated. Then the dense point clouds and ortho-rectification is thus generated, correspondingly ([Figure 2](#) – top left). Finally, a 'realistic photo-textured 3D model' is a direct output. For instance, [Figure 2\(c\)](#) illustrates the details of the eroded gullies situated on the westernmost massive mudstone (Lichi Mélange), which plays as an example of the quality of the dataset generated of the study area.

2.2. Update geological mapping through photo-interpretation on the high-resolution topographic data on the Pingting terraces

In order to update the mapping geology of the Pingting area, we used herein basic keys of photointerpretation (e.g. Howard 1967; Deffontaines & Chorowicz 1991; Deffontaines et al. 1992;

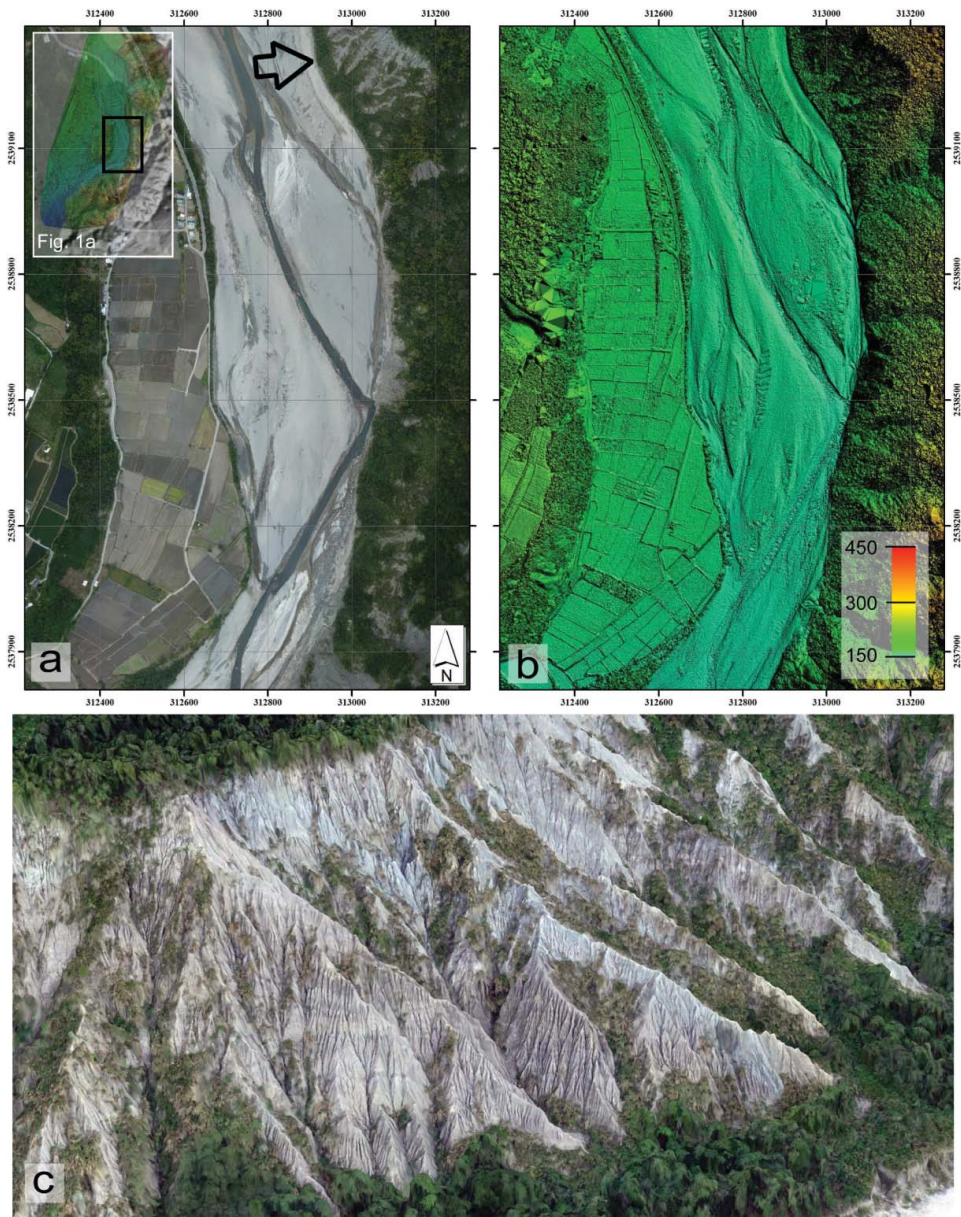


Figure 2. UAV Digital Terrain Model of the Pingting area. (a) Orthorectified photomosaic of the UAV Pingting area. (b) UAV triangular irregular network (TIN) coloured hill-shaded hypsometry. (c) Snapshot of the UAV DTM zoom-in 3D model of the study area where the eroded gully and strata are clearly identifiable from the image. The location of the scene is indicated by the black arrow marker plotted on [Figure 2\(a\)](#).

Deffontaines et al. 1993) by analysing the structures, and the textures of the DTM in order for instance to highlight homogenous areas that characterize same lithologies. We focus also on the drainage network geometry in order to get fault and folds, and drainage density and frequency to get permeabilities, as well as topographic slopes that gives hardness/softness of rocks (e.g. Howard 1967; Deffontaines & Chorowicz 1991; Deffontaines et al. 1992; Deffontaines et al. 1993; Pubellier et al. 1994). In order to more precisely locate the structural geometry of faults, particular attention was carried on the stratigraphic dip and the topographic chevrons and flat irons that reveal geological structures on the digital topography. We then are able to up-date and modify consequently geological mapping ([Figure 2\(b\)](#)) adding several items such as the well preserved paleo-surface (PS)

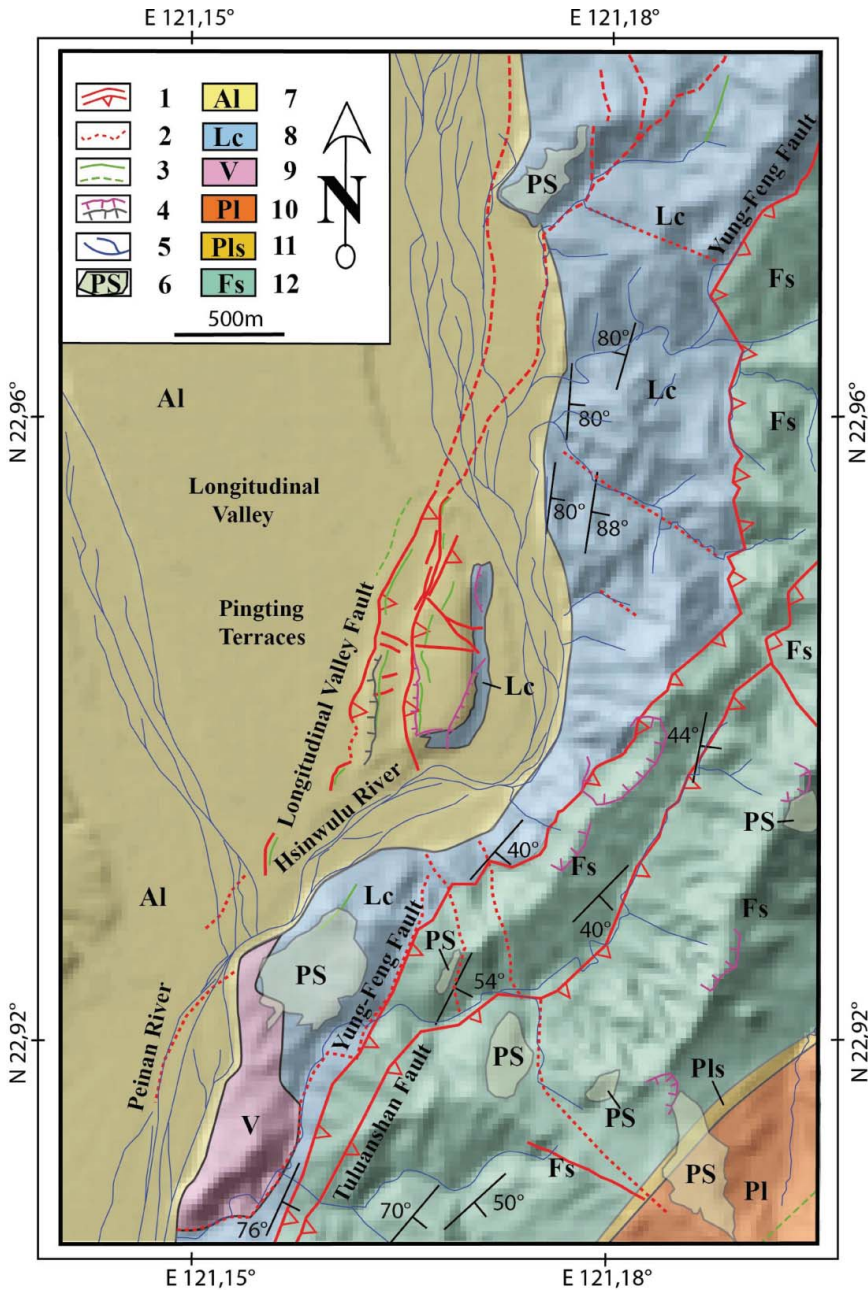


Figure 3. UAV's high-resolution DTM. (B) New structural and geological photo-interpretation from the high-resolution UAV DTM combined with pre-existing published geological mapping. One may note the up-dating structural geometry of both Pingting terraces as well as the western side of the Coastal Range: (1) Fault, (2) inferred fault, (3) fold, (4) landslide, (5) drainage network, (6) paleo surface, (7) alluvial deposit, (8) Lichi Mélange, (9) andesitic blocks within the Lichi Mélange, (10) Paliwan formation conglomerate facies, (11) Paliwan formation, and (12) Fanshuliao formation.

against active erosion, as well as the numerous faults splays that affect the topographic surface (e.g. the Pingting Terrace Fault 1 – PTF1 – and Pingting Terrace Fault 2 – PTF2 – of the Pingting terraces, see Figure 5). Some landslides crowns also were identified in the western part of the CoaR above the Hsinwulu river, within the Lichi Mélange that needs to be taken into account for the resulting structural geometry. Active vertical scarps without vegetation in the fields confirm the land-slidings.

Consequently, after this careful photo-interpretation geological and geomorphological mapping, the two Pingting terraces appear to be offset on their westward limb by faults with vertical component as the eastern terrace is uplifted relatively to the western one as already seen by previous authors (Shyu et al. 2008; Champenois et al. 2012).

In order to characterize and quantify the present tectonic activity of the new geological scheme of the Pingting area and their different units, we combine this approach with SAR interferometry (see below and following interferometric works of both Fruneau et al. 2001 and Pathier et al. 2003).

3. Multi-temporal InSAR analysis and Pingting PALSAR application

3.1. InSAR methods: MTI-StaMPS method

Since early 1990s, conventional Differential Synthetic Aperture Radar Interferometry (DInSAR) is usually employed to investigate surface deformation processes (e.g. Massonnet et al. 1994; Wright et al. 2001), but some limitations appear such as atmospheric phase delay or temporal decorrelation (Zebker & Villasenor 1992; Zebker et al. 1997). To address these limitations, two different approaches were developed in the early 2000's, both based on time series analysis, the Small Baseline InSAR (SBAS) (Berardino et al. 2002; Lanari et al. 2004) and the Persistent Scatterer InSAR (PSI) (Ferretti et al. 2001; Hooper et al. 2007). Those techniques, relying on a set of interferograms built from SAR data acquired at different times, allow to measure displacements on specific points at each date of SAR acquisition and over long period time. SBAS is based on interferograms formed with criteria of short time interval and small difference of perpendicular baseline (i.e. the component of the satellite separation distance that is perpendicular to the look direction) while PSI is based on interferograms formed with respect to one single image called 'Master Image.' Despite many advances in time series analysis, there are still limitations for measuring surface deformation processes especially in vegetated natural landscape and agricultural area where the temporal change of the ground can cause rapid signal decorrelation (e.g. Meng & Sandwell 2010). Moreover, corrections of the atmospheric phase screen in the interferograms are one major limitation. Among the present solutions to take it into consideration, there are global atmospheric models (e.g. Jolivet et al. 2011), the combination of spatio-temporal filters of the interferometric phase (Hooper et al. 2007), principal components analysis, and use of total zenithal delay derived from GPS measurements. Nonetheless, one recent advance in time series propose to combine PSI and SBAS approaches (Hooper et al. 2012). Indeed, the two approaches can be considered as complementary because they have not been developed for the same model of surface scattering. From there, it is possible to use them together to improve the spatial density of measurements and, when pixels are selected with both approaches, to improve the signal-to-noise ratio (Hooper et al. 2012).

In this study, the multi-temporal InSAR (MT-InSAR) algorithm developed by A. Hooper (2008) is used. Both information of amplitude dispersion, derived from Ferretti et al. (2001), and phase stability with time are used to determine which pixels can be considered as PS pixels or slowly-decorrelating filtered phase (SDFP) pixels for SB approach. Then a 3-D phase unwrapping (Hooper et al. 2007) is applied to the combined dataset and further processing for extracting the signal deformation are applied. This algorithm differs from other because full resolution interferograms are used for SB approach and no a priori model of deformation through time is used, but it assumes that deformation and consequently the interferometric phase is spatially correlated. At the end of the MT-InSAR processing chain, a map giving for each pixel its mean velocity along the radar line of sight (over the whole period) and a time series of displacements at each acquisition date are obtained.

3.2. Pingting PALSAR data

A set of nine PALSAR (Phase Array type L-band Synthetic Aperture Radar) data provided by the ALOS satellite from the Japan Aerospace Exploration Agency (JAXA) acquired between January

Table 1. Information of the PALSAR images from Path 445, Frame 440 of ALOS.

Image no.	Year	Month	Day	Baseline ^a (m)	Time ^b (days)	Category of image
1	2007	01	29	−1504	0	Slave
2	2007	08	01	−277	184	Slave
3	2007	09	16	−430	230	Slave
4	2007	12	17	0	322	Master
5	2008	05	03	862	460	Slave
6	2009	08	06	−1572	920	Slave
7	2009	12	22	−638	1058	Slave
8	2010	02	06	−234	1104	Slave
9	2010	09	24	592	1334	Slave

^a Perpendicular baseline component.

^b Time difference relative to the master image.

2007 and September 2010 is used in this study (Table 1). One major characteristic of the PALSAR sensor is that it operates in L-band, with a wavelength (23.6 cm) five times longer than the wavelength of usual C-band sensors commonly employed for Synthetic Aperture Radar Interferometry (InSAR) studies. The heading angle (or azimuthal angle) is about 13° to the West and the mean incidence angle is 38.7°. Recent studies have demonstrated the improvement of InSAR results quality using L-band data over area with tropical and dense vegetation cover (e.g. Meng & Sandwell 2010; Champenois et al. 2012) due to a higher penetrative capacity. PALSAR data used in this study are from the ascending path 445 and cover the southern part of the Longitudinal Valley from Ruesuei to Taitung (which is actually the most active), but in this paper we only focused on the Pingting Terraces.

3.3. Spatial analysis of interseismic creep activity

Using the dataset described previously, eight interferograms for the PS method and 16 interferograms for the SB method were formed (Figure 4), which gives coherent results despite the few number of resulting interferograms (see Hooper et al. 2007). It is clear that a reduced amount of dataset reduces a bit the accuracy of our PS InSAR measurements. Dealing with the critical baseline parameter (spatial component), we choose 1100 m, and we choose 930 days for the temporal baseline, these two values seem reasonable for L-band data for such area of Taiwan. Concerning the differential interferograms, the PS approach has also been developed to exploit interferograms with low coherence. As in StaMPS, full interferograms are just used at the beginning of the process, one of its interest is that even on interferograms that look noisy (clearly difficult to read) it is possible to extract pixel information on surface displacements. We considered herein a 40 m DEM derived from optical data for the generation of the DInSAR results, which is reasonable to remove the topographic component in these ALOS interferograms. The chosen ‘Master Image’ for PS processing is the 17/12/2007 SAR acquisition. At the end of both processes, applying the same selection threshold (0.4, which is given as a reasonable value by Hooper et al. 2007) and the same per cent of pixels with random phase accepted (10%), 3600 pixels were identified with the PS method, whereas with the SB method 2800 pixels were identified. Finally, more than 6400 pixels were selected over this 53 square kilometres rural area leading to a density of measurements of about 120 pixels/km². This density value is a significant improvement compared to the Peyret et al. (2011) study using ERS SAR C-band data and the Champenois et al. (2012) study using only PS method with ALOS PALSAR L-band data.

Results from the combined method are shown in Figure 5(a). The western part, corresponding to the Longitudinal Valley, presents a higher pixel density compared to the eastern part mainly due to the presence of dense vegetation and high topography. However, the spatial sampling of measurements over the CoAR is enough to analyse the interseismic surface deformation for the 2007–2010 period over the Pingting Terraces. The reference area used in this study is a city located West to the

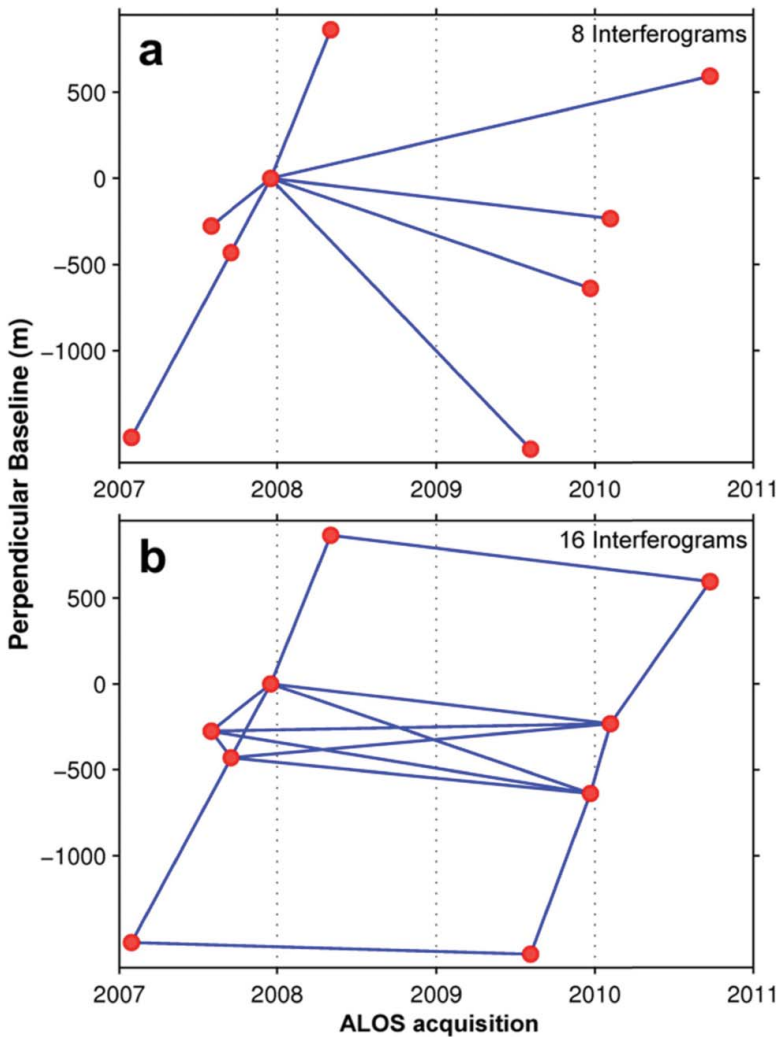


Figure 4. Baseline plot for (a) the persistent scatterer method and (b) the small baseline approach. The red dots represent PALSAR images, while the blue lines indicate the interferograms that are formed. The perpendicular baseline corresponds to the component of the satellite separation distance that is perpendicular to the look direction.

Pingting terraces and close to the profile BB'. The MT-InSAR results show localized deformations that are consistent with shallow creep reaching the surface. At first glance, two blocks with relative differential displacement can be distinguished: the westward one corresponding to the Longitudinal Valley with mean LOS velocities close to 0, and the eastward one corresponding to the CoaR which is rapidly uplifting and overthrusting with mean LOS velocities ranging from +10 mm/yr to +35 mm/yr toward the satellite. Between these blocks, two active fault sections can be precisely localized, characterized and quantified. They correspond to the Pingting Terraces Faults (PTF1 and PTF2, see [Figure 5\(a\)](#) and [5\(b\)](#)). Separated by only 250 m average, they are parallel to each other and N020°E trending as the LVF orientation.

North of the study area (Latitude: 22.975°N), a first discontinuity in mean LOS velocities is localized at the basal relief of the western side of the CoaR and can be associated with the LVF. Eastward, another discontinuity in mean LOS velocities is localized inside the CoaR. Contrary to other places of the southern Longitudinal Valley, the total deformation is there accommodated by two active

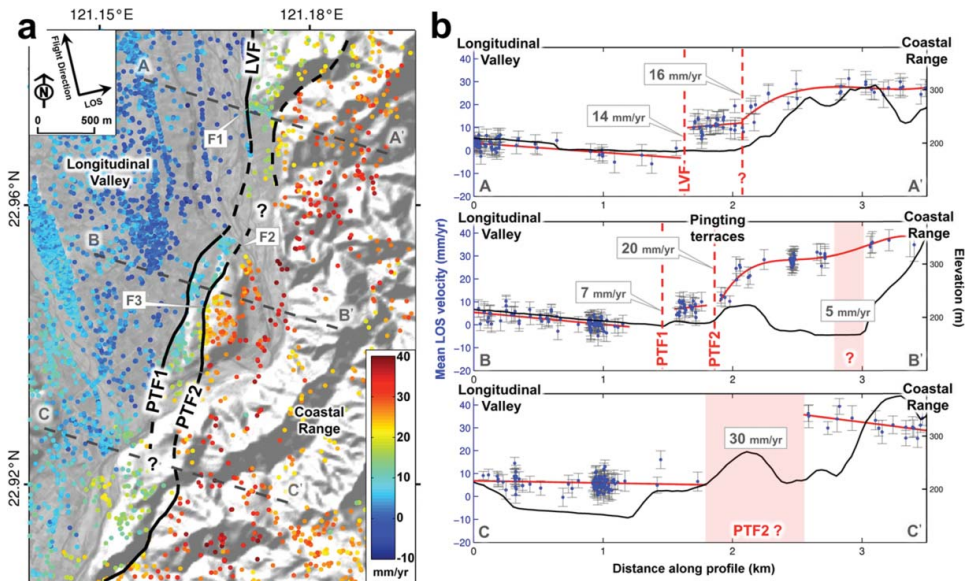


Figure 5. (a) Mean line-of-sight velocity map for the Pingting Terraces area from combined MT-InSAR method. The black lines represent update detailed fault traces obtained with the MTI results and grey dashed lines indicate the location of the three mean LOS displacement profiles presented on the right. On the left top corner, two arrows indicate the flight direction of ALOS satellite associated with ascending track, and look direction of radar (line of sight). Labels F1, F2 and F3 indicate marker of deformations found during field investigations and shown in Figure 8. LVF: Longitudinal Valley Fault; PTF1: Pingting Terraces Fault 1; PTF2: Pingting Terraces Fault 2. (b) Mean line-of-sight velocity profiles. All profiles are perpendicular to the major active segments they cross. Each profile is superimposed on the topographic profile from a 40 m Digital Terrain Model. Estimated LOS displacement rates of each fault are indicated in grey.

structures: the LVF (PTF1 and PTF2) and a ‘continuous’ active deformation within the Lichi Mélange that is deduced in this study based on the MT-InSAR our result especially the motion profiles (see Figure 5(b)).

To quantify and analyse creeping activity of faults, we choose to estimate the total LOS velocity offsets (LOSVOs). To calculate the total LOSVO between both sides of the faults, the hangingwall and the footwall are separated according to each fault traces and a regression (linear or polynomial regression of order from 1 to 3) is performed on each side. By the way, the width of the profiles lines used is 100 m (50 m on each side). Afterward, the LOS velocities are computed to the nearest fault trace for both side and used to estimate the total LOSVO across the fault. The mean value of uncertainty associated with all LOSVO values is about 3 mm/yr taking into account both sides of the faults the standard deviation of uncertainties associated with each PS (StaMPS outputs) nearest of the fault. Then we estimated the mean of these two values (one for the West side and one for the East side of the fault).

Using the Profile AA’ (Figure 5(b)), LOSVO associated with the LVF and the new fault are, respectively, 14 mm/yr and 16 mm/yr. Moreover, this profile gives significant information about the depth of creep by simply analysing the surface deformation (clear discontinuity or distributed LOS velocities on surface). For the LVF, it appears that the fault creeps up the surface because the deformation occurs within 100–200 m while the one associated with the other fault is less localized over more than 500 m. The fault located inside the CoaR is not precisely localized moving southward and its trace is completely lost when approaching the Peinan River which presents a low density of point of measurement. Regarding the LVF, it appears that the fault crosses the river until the Pingting Terraces and becomes the Pingting Terraces Fault 1 (PTF1).

Over the Pingting terraces, significant gradients of mean LOS velocity appear close to the two major western basal reliefs of the terraces. In the Profile BB’ (Figure 5(b)), it arises that these

gradients are associated with the interseismic creep activity of the Pingting Terraces Faults 1 and 2 (PTF1 and PTF2) with, respectively, 7 mm/yr and 20 mm/yr of LOSVO. The poor density of points west to the PTF1 does not allow interpreting the surface deformation whereas the surface deformation associated with the PTF2 is localized over more than 400 m. Eastward of the PTF2, a small offset in mean LOS velocities can be observed at the western foot of the CoaR. With a 5 mm/yr LOSVO, this gap can be associated with another active tectonic structure branching at depth one of the two Pingting Terraces Fault. However, without more information, it is difficult to map and study in detail this hypothetical structure.

In the southern part of the study area, the mean LOS velocity map reflects a more complex tectonic setting. Indeed, the PTF1 trace is slowly disappearing inside the Peinan River mainly due to the weak density of point of measurement as mentioned before, whereas the PTF2 seems to pass through the CoaR (over more than 3 km) and joins more southerly the Longitudinal Valley. The Profile CC' (Figure 5(b)) shows a substantial offset in LOS velocities across the PTF2 of about 30 mm/yr. However, fault trace cannot be correctly localized with no point of measurement over more than 800 m around the fault.

3.4. Spatial and temporal analysis of LVF interseismic creep activity during 2007–2010

The MT-InSAR method permits a temporal analysis thanks to a time series of measurement with one value of deformation for each SAR data used in the process. The first aim of a temporal analysis is to investigate the linear and the non-linear components of the interseismic creep activity. Figure 6 (a) presents the time series of LOS displacement over the Pingting Terraces with respect to the older SAR acquisition (29/01/2007). The deformation appears to be linear with time and only the 22/12/2009 seems to present a problem with lower values of displacement overall the study area. This problem could be due to the presence of an atmospheric artefact that has not been correctly removed during the MT-InSAR processing. In order to remove atmospheric artefact, we used the spatio-temporal filters developed and available in StaMPS. These have been parametrized with the following values: spatial grid size of 300 m and temporal grid size of 730 days.

In order to examine the temporal variation of shallow creeping activity of the PTF1 and PTF2, the Profile BB' is used to estimate cumulate LOS Displacement Offset with time (Figure 6(b)). As the LOS Displacement Offset is estimated on a short distance (hundreds of metres), this parameter is less sensitive to atmospheric perturbations which show typical variations at large wavelength. Both faults present a linear temporal deformation with slight variations, which are within the error bars. The total LOS displacement across the Pingting Terraces occurs with a mean rate of about 26.6 mm/yr.

3.5. InSAR deformation mapping and field investigations

Two previous studies established a local structural map of the terraces based on geomorphological analysis (Shyu et al. 2008, Figure 1(c)) and on PS InSAR analysis (Champenois et al. 2012, Figure 1(c)). However, some fault traces were still unclear, especially the northern part of the terraces with a probable connection to the LVF. The high density of point of measurement obtained with the MT-InSAR method allows updating more accurately shallow creeping sections of the faults. The resulting fault traces are shown in Figure 5(a) and can be compared to the map of Shyu et al. (2008, Figure 1(c)). Some disparities appear north and south of the terraces and can result from positioning error when only geomorphological approach is used over area subject to erosion or recent fluvial deposits (Chen et al. 2007).

To validate the MT-InSAR update faults map, two field trips have been conducted in the study area to locate evidences of surface deformation near the Pingting Terraces Faults and the LVF. Three evidences are presented in Figure 7 and can be easily localized in Figure 5(a). North of the Pingting Terraces, clear evidence of tectonic activity is localized on the Paohua Bridge which crosses the Hsinwulu river perpendicularly to the LVF (Figure 7, F1). About 200 m from its eastern ends, this

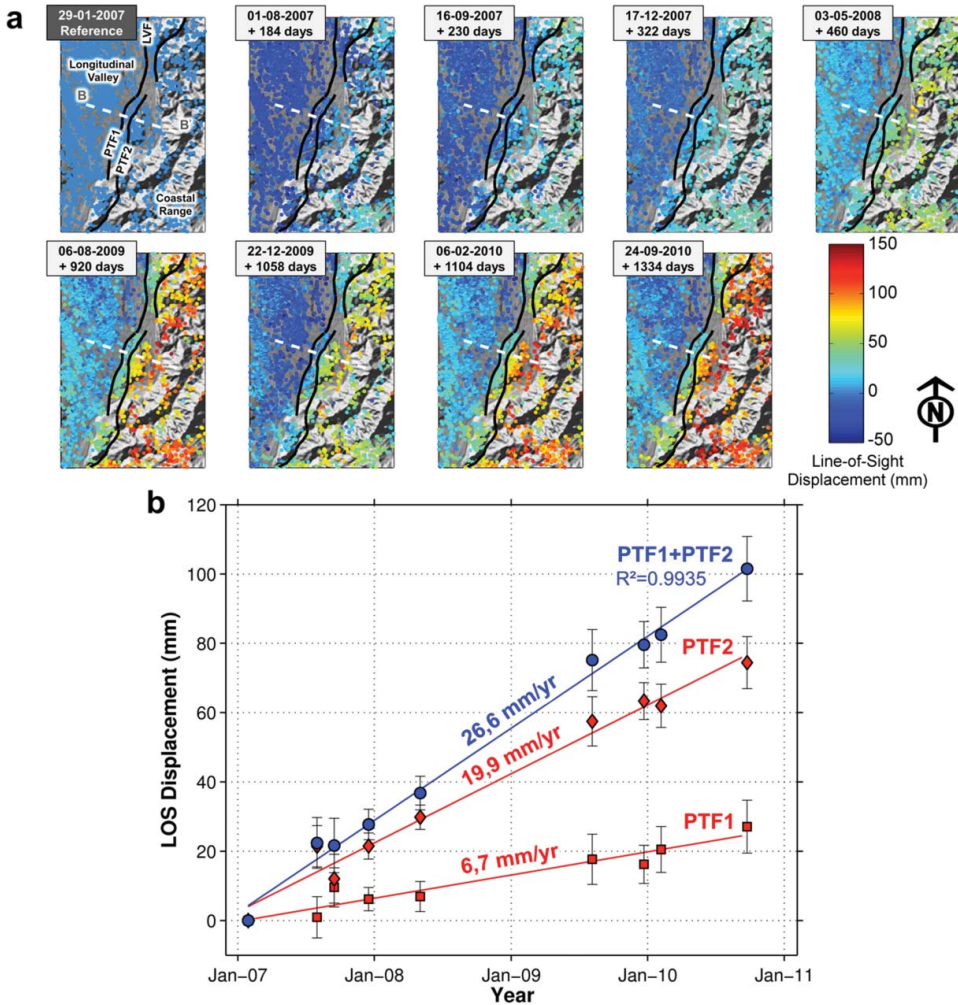


Figure 6. (a) Time series of line-of-sight displacement over the Pingting Terraces area from combined MT-InSAR method. The black lines represent update detailed fault traces obtained with the MTI results and the white dashed line shows the profile used for the (b) temporal evolution of line-of-sight displacement across the Pingting Terraces Faults. The red lines are linear regression associated with the Pingting Terraces Faults and the blue line is linear regression for the sum of the two Pingting faults.

bridge is affected by the vertical component activity of the LVF where the eastern part is uplifting compared to the western part which appear to be stable in the InSAR monitoring 2007–2010 period of time. Southward, guided by the MT-InSAR map, two evidences were found close to the PTF2. Marker of deformation F2 (Figure 7) illustrates the thrust component of fault slip across a concrete dike over its entire height. Furthermore, evidence F3 occurs on a channel close to the Profile BB' where the estimated LOSVO is about 20 mm/yr. In this place, the eastern part is thrusting and offset the drainage channel.

4. Discussions

4.1. The Pingting shallow interseismic deformation

It is of prime importance to superimpose both surface displacements deduced from InSAR and the geological framework on the Pingting area. That reveals the structurally active places such

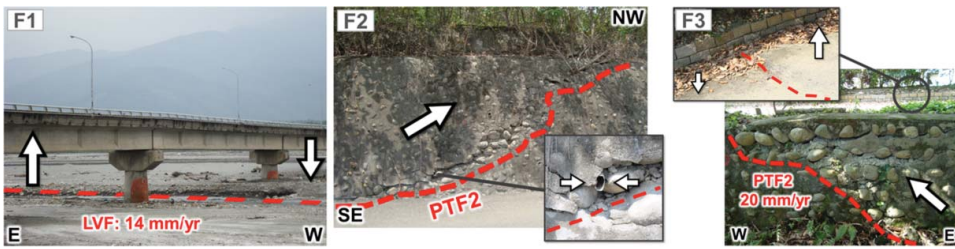


Figure 7. Field evidences of tectonic activity over the Longitudinal Valley Fault (LVF) and the Pingting Terraces Fault 1 (PTF1) (see location in Figure 5(a)). F1 – the Paohua Bridge: the bridge is deformed by the activity of the Longitudinal Valley Fault (Fault); its eastern part is uplifting contrary to its western one which appears stable toward the LOS. F2 – Pingting concrete dike: the deformation in this place reveals a clear thrust component of the PTF2 fault displacement, scale 10 m. F3 – Pingting channel: the PTF2 thrust fault cross obliquely a river channel and destructed it, scale 5 m. A small compressive pop-up bounded by two reverse faults is seen in the lateral concrete dikes, scale 3 m.

as the relative subsidence or surrection areas as well as active faults and folding during the 2007–2010 time period that have a differential displacement toward the line of sight.

One may note that the LVF zone is composed of two branches from north to south that are both interseismically active and have a differential structural behaviour. Figure 8 reveals the interseismic displacement where one may notice west of the LVF the relative subsidence of the Longitudinal Valley (toward the CoaR), that acts as the drag fold linked to the thrusting activity. Eastward of the LVF, the maximum uplifting rate relatively to the LOS is situated within the Lichi Mélange highlighting the ductile behaviour of the Lichi Mélange toward the present compression. The uplift axis turns slightly southward to the SE within the Fanshuliao volcanic Formation (Fc) of the Luzon volcanic arc (see heavy green line of Figure 8).

From the InSAR map of LOS displacement (Figure 5(a)), we may characterize differently the two splays that branches close to the surface PTF1 and PTF2 on the Pingting terraces as well as the differential displacement due to the geometry at depth. PTF1 appears to be a flatter thrust and may correspond to a front shortcut thrusting fault, than the deeper dipping PTF2, east of which active folding occurs (Figure 9).

Therefore, a local partitioning is evidenced herein close to the surface. During the 2007–2010 interseismic time period, PTF1 is an active creeping thrust contrasting with PTF2 that acts as the thrust base of an active anticline. Due to the northern and southern geometry, we infer that both connect at depth in only one major fault 50° dipping and corresponding to the LVF (see Hu et al. 2007).

4.2. The Longitudinal Valley Fault and the coastal range geological and geodynamic regional implications

The interseismic tectonic evolution of the CoaR shows a dissymmetric tilting, higher surrection to the west contrasting to a lower one to the east (Barrier & Muller 1984; Angelier et al. 1997) by its overthrusting above the Longitudinal Valley (Figure 10). One may notice that the maximum interseismic deformation deduced from InSAR results occur on the eastern part of the Longitudinal Valley, close to the CoaR. There the Hsinwulu/Peinantahsi rivers flow within the maximum subsiding area. The maximum displacement occur within the Lichi Mélange in between the LVF that is characterized in the Pingting area by two splays (PTF1 acting as an interseismic active west vergent thrust and PTF2 acting as the thrust below an active folding structure). The displacement develops and increases further east within the Lichi Mélange and may correspond to ejection of the lichi melanges beneath the CoaR series. The latter is so highly deformed and appear to be locally tightly folded within the fault zones (dip close to 80°).

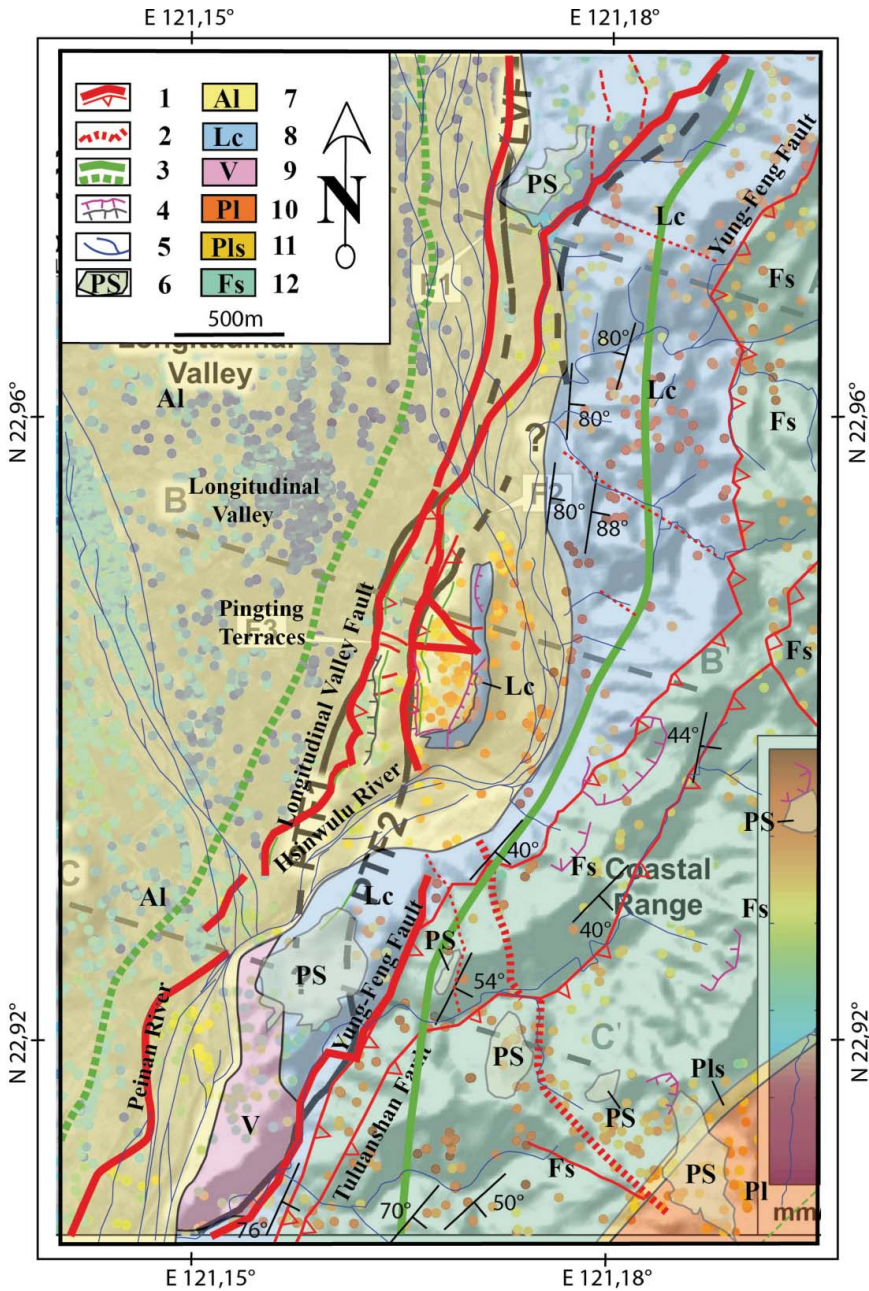


Figure 8. Resulting active interseismic structures deduced from the up-date geological mapping (with INSAR dots [Figure 5\(a\)](#)), of the Pingting area. Note the heavy red lines which act as active tectonic thrust faults west verging and heavy green line that correspond to the maximum uplift area and in heavy dashed green line the maximum relative subsidence of the place. Low right corner: Mean LOS velocity derived from InSAR (scale bar purple – 10 mm/y; red – 40 mm/y).

Within the CoaR few different deformations occur as it is just passively transported with a slight tilt to the east (see East [Figure 10](#)). Furthermore, from this InSAR result, the Tuluanshan and the Yung-Feng thrust faults, do not present characteristic displacements toward the LOS during the 2007–2010 time period and with this wavelength. Of course these faults may be blocked and needs a longer time period, a longer wavelength to precise their possible interseismic displacements.

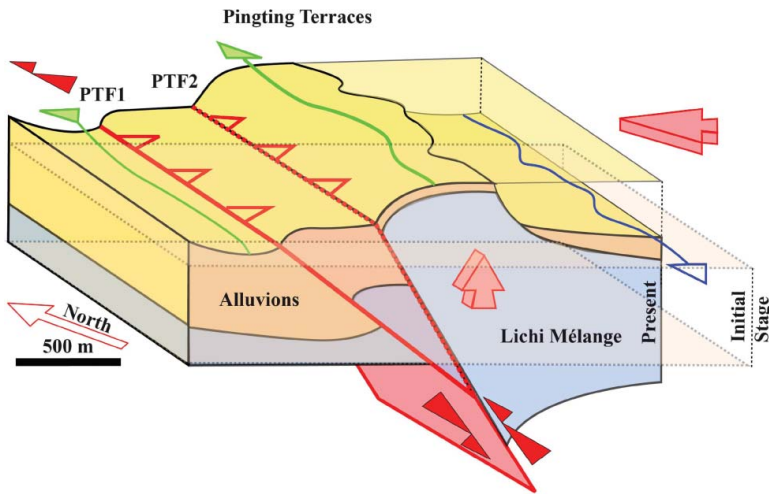


Figure 9. 3D schematic structural view of the Pingting terraces deduced from both detailed photo-interpretation and update geological mapping as well as InSAR displacement along the LOS.

Furthermore active oblique or horizontal displacement toward the LOS may also occur that will be difficult to decipher from this InSAR result. It should be interesting to date precisely the remnants of the CoAr Paleo Surfaces (PS: item 6 of Figure 3) revealed by the photo-interpretation of the so precise DTM in order to reconstruct the longer term of the neotectonic deformation.

From the geomorphic point of view, the Hsinwulu river flows southward generally guided by both the active syncline (drag fold of the LVF) and along the LVF. In the Pingting terraces vicinity it flows within the ‘anticline deformation’ within the soft clayey Lichi mélange (Lc) revealing this superimposition of drainage to tectonic activities which has been possible due mainly by the softness of the highly deformed Lichi Mélange, a good example for differential erosion applied to active tectonics.

One may notice that our active tectonic interseismic analyses and interpretations (active folds and faults) is done in the Pingting area (herein) without taking into account the possible co- and post- seismic effects, such as those due to the (Mw 6.8) Chengkung earthquake (2003 – which epicentre is situated at around 20km to the NE), that had definitely affected the area (see Hu et al. 2007). Effectively, as regard to the seismological catalogue provided by the Taiwanese Central Weather Bureau (CWB), no shallow earthquake with significant magnitude occurred during the

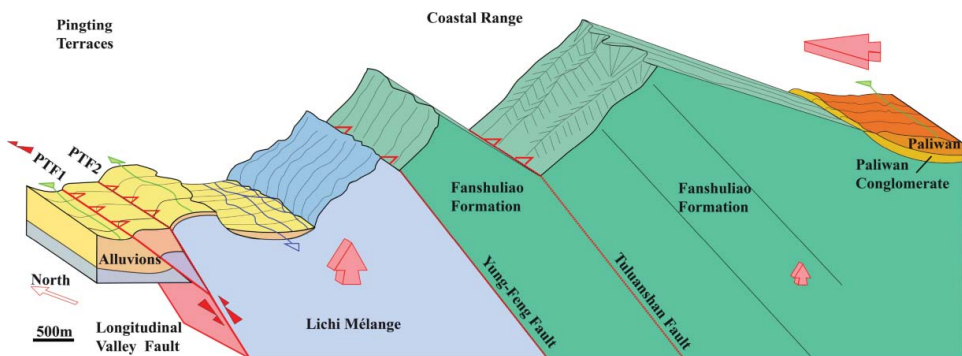


Figure 10. 3D schematic view of the Pingting terraces and the western Coastal Range. The red lines represent the Pingting terraces faults with the line-of-sight displacements estimated in this study. The red arrow on the right top corner indicates the direction of convergence between the Philippine Sea Plate and the Eurasian Plate with an estimated rate of about 82 mm per year (Seno et al. 1993).

studied period of this paper. Unfortunately, there is an only one continuous GPS station to monitor the Pingting terraces (ERP, Hu et al. 2007), it shows coherent and convergent results even if the so small amount of stations makes it difficult to compare those to our InSAR results (Champenois et al. 2012). The Longitudinal Valley appears to be stable and not displaced comparing to the general surrection of the CoaR.

5. Conclusions

Over the Pingting Terraces, the use of both high-resolution topographic data combined with previous geological maps, allow us mapping more precisely the structural geometry of the major suture of the Eurasian/Philippine sea plate collision within the Longitudinal Valley. Furthermore InSAR time series interferometry in between 2007 and 2010 helps to characterize and quantify the interseismic present displacements. Therefore, the LVF, in the Pingting terraces vicinity, is not accommodated by only one structure as it is the case northward in the Yuli or Fuli area (see Champenois et al. 2012) but by two fault splays that connect at depth due to their field geometry. On the InSAR deformation cross-sections perpendicular to the LVF, it appears clearly that the western branch (PTF1) corresponds to an outcropping flatter thrust fault west verging without folding component, and is interpreted as a shortcut of the thrusting propagation of the active deformation. Whereas the eastern branch (PTF2) seems to be locked at the surface and corresponds to a thrust below an active fold west verging with a much higher rate (x3). Therefore, we interpret the PTF2 eastern splay as deeper than the western one (PTF1). PTF2 may be the surface trace of the buried LVF. So tectonic partitioning prevail in that area of the Longitudinal Valley. It is difficult to estimate the lateral strike-slip displacement without a local GPS network but due to its geometry it is inferred much less important than the vertical thrusting component. The whole active deformation appears to focus on the Lichi Mélange which act as a ductile mobile layer to the compression that concentrate the vertical uplift due to the vertical extrusion and ejection of the material. The CoaR generally is passively transported and slightly tilted as it is transported and overthrust above the Longitudinal Valley. Moreover, we reveals remnants of paleo-surface within the CoaR that should be interesting to date precisely (see PS: item 6 of Figure 3) revealed by the photo-interpretation of the so precise DTM in order to reconstruct the longer term of the neotectonic deformation. We then are able to quantify locally with good confidence the inter-seismic deformation of the LVF that have also major implications on the present CoaR geometry. It is of high importance to monitor these active tectonics displacements in order to prevent and to better understand the future LVF Earthquakes. We therefore are able to propose a structural geometry and a quantification of the inter-seismic active displacements of the LVF and the western part of the CoaR close to the Pingting terraces.

Acknowledgements

We are grateful to A. Hooper for having developed and permitting use of the 'StaMPS/MTI' algorithms and Samuel Magalhaes for the representation of interferometric cross-sections. A word of thanks also goes to the constructive remarks of both reviewers.

Disclosure statement

No potential conflict of interest was reported by the authors.

Funding

This research was supported for the UAV survey by the Central Geological Survey of Taiwan (MOEA – PI Chang Kuo-Jen) and for the SAR analyses by the Japan Aerospace Exploration Agency (JAXA) in the scope of PI 112-0001 project (project number: 5226904000 Benoît Deffontaines and Hu Jyr Ching). The authors thank LIA ADEPT/D3E and CNRS/NSC for funding part of the field trips.

ORCID

Benoît Deffontaines  <http://orcid.org/0000-0001-5104-8264>

References

- Angelier J, Chu HT, Lee JC. 1997. Shear concentration in a collision zone: kinematics of the Chihshang fault as revealed by outcrop-scale quantification of active faulting, Longitudinal Valley, eastern Taiwan. *Tectonophysics*. 274:117–143.
- Barrier E, Muller C. 1984. New observation and discussion on the origin and age of the Lichi Mélange. *Mem Geol Soc China*. 6:303–326.
- Berardino P, Fornaro G, Lanari R, Sansosti E. 2002. A new algorithm for surface deformation monitoring based on small baseline differential SAR interferograms, *IEEE Trans Geosci Remote Sens*. 40:2375–2383.
- Champenois J, Fruneau B, Pathier E, Deffontaines B, Lin KC, Hu JC. 2012. Monitoring of active tectonic deformations in the Longitudinal Valley (Eastern Taiwan) using persistent scatterer InSAR method with ALOS PALSAR data. *Earth Planet Sci Lett*. 337–338:144–155.
- Chang CP, Angelier J, Huang CY. 2000. Origin and evolution of a mélange: the active plate boundary and suture zone of the Longitudinal Valley, Taiwan. *Tectonophysics*. 325:43–62.
- Chi W-C, Chen L, Liu CS, Brookfield M. 2014. Development of arc-continent collision mélanges: linking onshore geological and offshore geophysical observations of the Pliocene Lichi Mélange, Southern Taiwan and northern Luzon arc, Western pacific. *Tectonophysics*. 636:70–82.
- Chen W-S, Yen IC, Fengler KP, Rubin CM, Yang, C-C, Yang H-C, Chang H-C, Lin C-W, Lin W-H, Liu Y-C, Lin Y-H. 2007. Late Holocene paleoearthquake activity in the middle part of the Longitudinal Valley fault, eastern Taiwan. *Earth Planet Sci. Lett*. 264:420–437.
- Deffontaines B, Chorowicz J. 1991. Principle of drainage basin analysis from multisource data: application to the structural analysis of the Zaire Basin. *Tectonophysics*. 194:237–263.
- Deffontaines B, Chotin P, Ait Brahim L, Rozanov, M. 1992. Investigation of active faults in Morocco using morphometric methods and drainage pattern analysis. *Geologische Rundschau, Stuttgart* 81 1:199–210.
- Deffontaines B, Pubellier M, Rangin C, Quebral R. 1993. Discovery of an Intra-arc transform zone in Mindanao (Philippines) using morphotectonic data, *Zeitschrift für Geomorphologie. Berlin – Stuttgart. Suppl.-Bd*. 94:261–273.
- Ferretti A, Prati C, Rocca F. 2001. Permanent scatterers in SAR interferometry. *IEEE Trans Geosci Remote Sens*. 39:8–20.
- Fruneau B, Pathier E, Raymond D, Deffontaines B, Lee C.T., Wang HT, Angelier J, Rudant JP, Chang CP. 2001. Uplift of Tainan Tableland (SW Taiwan) revealed by SAR interferometry. *Geophys Res Lett*. Vol. 28, N°16:3071–3074pp. doi:10.1029/2000GL012437.
- Ho, C.S. 1986. A synthesis of geological evolution of Taiwan. *Tectonophysics*. 125:1–16.
- Hooper A. 2008. A multi-temporal InSAR method incorporating both persistent scatterer and small baseline approaches. *Geophys Res Lett*. 35:L16302.
- Hooper A, Bekaert D, Spaans K, Arikani M. 2012. Recent advances in SAR interferometry time series analysis for measuring crustal deformation. *Tectonophysics*. 514–517:1–13.
- Hooper A, Segall P, Zebker H. 2007. Persistent scatterer interferometric synthetic aperture radar for crustal deformation analysis, with application to Volcán Alcedo, Galápagos. *J Geophys Res*. 112:B07407.
- Howard AD 1967. Drainage analysis in geologic interpretation: a summation. *Bull Am Ass Petr Geol Tulsa*. 51 (11):2246–3428.
- Hsu T.L. 1956. Geology of the coastal Range, Eastern Taiwan. *Bull Geol Surv Taiwan* 25:53–62.
- Hu JC, Cheng LW, Chen HY, Wu YM, Lee JC, Chen YG, Lin KC, Rau RJ, Kuo Chen H, Chen HH, Yu SB, Angelier J. 2007. Coseismic deformation revealed by inversion of strong motion and GPS data: the 2003 Chengkung earthquake in eastern Taiwan. *Geophys J Int*. 169:667–674.
- Huang MJ, Chang KJ. 2014. Unmanned aerial vehicle (UAV) associated DTM quality evaluation and application. *Mag Chinese Inst Civil Hydraulic Eng*. 41(4):52–58. (in Chinese with English abstract).
- Huang CY, Chien CW, Yao B, Chang CP. 2008. The Lichi Mélange: a collision mélange formation along early arcward backthrusts during fore-arc basin closure Taiwan arc-continent collision. *Geol Soc Am Spec Paper* 436:127–154.
- Jolivet R, Grandin R, Lasserre C, Doin M-P, Peltzer G. 2011. Systematic InSAR tropospheric phase delay corrections from global meteorological reanalysis data. *Geophys Res Lett*. 38:L17311. doi:10.1029/2011GL048757.
- Lanari R, Mora O, Manunta M, Mallorqui JJ, Berardino, P, Sansosti, E. 2004. A small-baseline approach for investigating deformations on full-resolution differential SAR interferograms. *IEEE Trans Geosci Remote Sens*. 42:1377–1386.
- Lee JC, Angelier J, Chu HT, Hu JC, Jeng FS. 2001. Continuous monitoring of an active in a plate suture zone: a creepmeter study of the Chihshang fault, eastern Taiwan. *Tectonophysics* 333:219–240.

- Lee JC, Angelier J, Chu HT, Hu JC, Jeng FS, Rau RJ. 2003. Active fault creep variations at Chihshang, Taiwan, revealed by creep meter monitoring, 1998-2001. *J Geophys Res.* 108:2528. doi:10.1029/2003JB002394.
- Malavieille J, Lallemand SE, Dominguez S, Deschamps A, Lu C-Y, Liu C-S, Schnurle P, Angelier J, Collot JY, Deffontaines B, Fournier M, Hsu SK, Le Formal JP, Liu SY, Sibuet JC, Thareau N, Wang, F, Crew TAS. 2002. Arc-continent collision in Taiwan: new marine observations and tectonic evolution. *Geol Soc Am Spec Papers.* 358:187–211.
- Massonnet D, Feigl K, Rossi, M, Adragna, F. 1994. Radar interferometric mapping of deformation in the year after the landers earthquake. *Nature* 369:227–230.
- Meng W, Sandwell DT. 2010. Decorrelation of L-band and C-band interferometry over vegetated areas in California. *IEEE Trans Geosci Remote Sens.* 48:2942–2952.
- Pathier E, Fruneau B, Deffontaines B, Angelier J, Pai CC, Yu SB, Lee CT. 2003. Coseismic displacements of the footwall of the Chelungpu fault caused by the 1999, Taiwan, Chi-Chi earthquake from InSAR and GPS data. *Earth Planet Sci Lett.* 212:73–88.
- Peyret M, Dominguez S, Cattin R, Champenois J, Leroy M, Zajac A. 2011. Present-day interseismic surface deformation along the Longitudinal Valley, eastern Taiwan, from a PS-InSAR analysis of the ERS satellite archives. *J Geophys Res.* 116:B03402.
- Pubellier M, Deffontaines B, Quebral R, Rangin C. 1994. Drainage network analysis and tectonics of Mindanao, Southern Philippines. *Geomorphology.* 9:325–342.
- Seno T, Stein S, Gripp AE. 1993. A model for the motion of the Philippine Sea Plate consistent with NUVEL-1 and geological data. *J Geophys Res.* 98:17941–17948.
- Shyu JBH, Sieh K, Chen Y-G, Chuang RY, Wang Y, Chung L-H. 2008. Geomorphology of the southernmost Longitudinal Valley fault: implications for evolution of the active suture of eastern Taiwan. *Tectonics.* 27:TC1019.
- Teng LS, Lo HJ. 1985. Sedimentary sequences in the island arc settings of the Coastal Range, eastern Taiwan. *Acta Geol Taiwanica.* 23:77–79.
- Wang Y, Chen WS. 1993. Geological map of eastern Coastal Range, Central Geological Survey. scale 1:100,000.
- Wright T, Parsons B, Fielding E. 2001. Measurement of interseismic strain accumulation across the North Anatolian Fault by satellite radar interferometry. *Geophys Res Lett.* 28:2117–2120.
- Yu S-B, Kuo L-C. 2001. Present-day crustal motion along the Longitudinal Valley fault, eastern Taiwan. *Tectonophysics.* 333:199–217.
- Zebker HA, Rosen PA, Hensley S. 1997. Atmospheric effects in interferometric synthetic aperture radar surface deformation and topographic maps. *J Geophys Res.* 102:7547–7563.
- Zebker H, Villasenor J. 1992. Decorrelation in interferometric radar echoes. *IEEE Trans Geosci Remote Sens.* 950–959.